Cell Death & Differentiation (2019) 26:502–515
https://doi.org/10.1038/s41418-018-0151-2

Cell Death & Differentiation

ARTICLE

Transient inhibition of p53 homologs protects ovarian function from two distinct apoptotic pathways triggered by anticancer therapies

So-Youn Kim[1] · Devi M. Nair[2] · Megan Romero[1] · Vanida A. Serna[2] · Anthony J. Koleske[3] · Teresa K. Woodruff[1] · Takeshi Kurita[2]

Received: 10 February 2018 / Revised: 17 May 2018 / Accepted: 18 May 2018 / Published online: 9 July 2018

Abstract

Platinum-based chemotherapies can result in ovarian insufficiency by reducing the ovarian reserve, a reduction believed to result from apoptosis of immature oocytes via activation/phosphorylation of TAp63α by multiple kinases including CHEK2, CK1, and ABL1. Here we demonstrate that cisplatin (CDDP) induces oocyte apoptosis through a novel pathway and that temporary repression of this pathway fully preserves ovarian function in vivo. Although ABL kinase inhibitors effectively block CDDP-induced apoptosis of oocytes, oocytic ABL1, and ABL2 are dispensable for damage-induced apoptosis. Instead, CDDP activates TAp63α through the ATR > CHEK1 pathway independent of TAp63α hyper-phosphorylation, whereas X-irradiation activates the ATM > CHEK2 > TAp63α-hyper-phosphorylation pathway. Furthermore, oocyte-specific deletion of *Trp73* partially protects oocytes from CDDP but not from X-ray, highlighting the fundamental differences of two pathways. Nevertheless, temporary repression of DNA damage response by a kinase inhibitor that attenuates phosphorylation of ATM, ATR, CHEK1, and CHEK2 fully preserves fertility in female mice against CDDP as well as X-ray. Our current study establishes the molecular basis and feasibility of adjuvant therapies to protect ovarian function against two distinctive gonadotoxic therapeutics, CDDP, and ionizing radiation.

Introduction

Genotoxic anticancer therapies often result in premature ovarian insufficiency (POI) by destroying the ovarian reserve, which represents all of the follicles available for future fertility and endocrine support. The current fertility preservation practices for female cancer patients primarily focus on the preservation of mature eggs or embryos externally. However, such approaches do not preserve the endocrine function of ovaries. Although transplantation of cryopreserved ovarian tissues may restore ovarian function in women with ovarian insufficiency, more than half of recipients do not resume their cycles or lose their cycles within few years [1–3]. As POI significantly compromises the quality of life with complications including infertility, osteoporosis, depression, anxiety, heart disease, and dementia, there remains an urgent need to maintain the ovarian functions of female patients, even in those who do not desire to bear a child. As an alternative to external preservation of ovarian tissues and embryos, adjuvant therapies that protect the ovarian reserve from off-target effects of anti-neoplastic agents have been intensively explored [4–10]. Although preclinical studies have shown promise, the mechanisms underlying the ovarian reserve protection by these adjuvants remain elusive.

Removal of damaged germ cells is an ancestral function of the p53 tumor suppressor family [11–13]. This evolutionally conserved role of p53 family genes reflects the

Edited by G. Melino

Electronic supplementary material The online version of this article (https://doi.org/10.1038/s41418-018-0151-2) contains supplementary material, which is available to authorized users.

✉ So-Youn Kim
so-youn-kim@northwestern.edu

✉ Takeshi Kurita
takeshi.kurita@osumc.edu

[1] Division of Reproductive Science in Medicine, Department of Obstetrics and Gynecology, Feinberg School of Medicine, Northwestern University, Chicago, IL, USA

[2] Department of Cancer Biology and Genetics, The Comprehensive Cancer Center, The Ohio State University, Columbus, OH, USA

[3] Department of Molecular Biophysics and Biochemistry, Yale University, New Haven, CT, USA

SPRINGER NATURE
CDDpress

significance of genomic surveillance by p53 homologs for the continuation of species [13–16]. Mammals carry three p53 paralogs, p53, p63, and p73, encoded by *TP53*/*Trp53*, *TP63*/*Trp63,* and *TP73*/*Trp73* in human/mouse [16], respectively. Knockout mouse studies have established a pivotal role for p63 in damage-induced apoptosis in primordial follicles (PFs) by ionizing radiation (IR) [17] and cisplatin (CDDP) [18]. The oocytes within PFs are highly sensitive to genotoxic insults due to the constitutive expression of TAp63α, an isoform of p63 [18–20]. TAp63α in healthy oocytes of PFs forms inactive dimers [21–23]. When DNA damage occurs, CHEK2 phosphorylates the transactivation inhibitory domain at S621, which in turn promotes the phosphorylation and formation of active tetramers in TAp63α [21, 24]. A study by Rinaldi and coworkers suggests that CHEK2 can be a target of ovarian reserve preservation: In ovarian organ culture, a CHEK2 inhibitor protected PFs from γ-irradiation, and the transplantation of these treated ovaries produced healthy pups [25]. A recent study by Tuppi et al. [26] has identified CK1 is an essential kinase that activates TAp63α via phosphorylation in response to DNA damage. The same study demonstrated that a CK1 inhibitor protects oocytes from DNA damage. In addition to CHEK2 and CK1, earlier studies by Gonfloni et al. [5] proposed c-ABL/ABL1 is one of the essential kinases that activate TAp63α, as ABL kinase inhibitors, imatinib and GNF-2, protected PFs from CDDP-induced apoptosis [27–29].

Although p53 is dispensable for IR-induced oocyte apoptosis [17], *Trp53* is required for the efficient removal of female germ cells that are defective in meiosis [24]. Female TAp73 null mice demonstrate defective spindle assembly in mature oocytes [30]. In addition, we previously demonstrated that TAp73 accumulates in the nucleus of CDDP-damaged oocytes within PFs [18]. Altogether, these observations suggest p53 homologs operate a multilayered safeguard system to protect the genomic integrity of the female germline. Furthermore, we identified differences in the phosphorylation patterns of TAp63α in oocyte apoptosis induced by IR and CDDP. Hence, in this study we further investigated the mechanisms of ovarian reserve loss caused by chemo- and radiotherapies.

Results

CDDP and X-ray activate TAp63α through distinctive pathways

ABL kinase inhibitors: imatinib, GNF-2 (Fig. 1a, b), nilotinib, and dasatinib (Figure S1a) dose-dependently protected up to 40% of PFs against CDDP but not from X-rays. In addition, hyper-phosphorylation of TAp63α, which was prominent in X-irradiated ovaries (Figure 1ci) was not induced by 4 μM CDDP (Figure 1cii), a concentration comparable to the plasma CDDP concentration of patients [31].

Although IR immediately causes DNA double-strand breaks (DDSBs), damage by CDDP gradually accumulates in the oocyte genome as the concentration of intranuclear CDDP rises. Therefore, the mobility shift of TAp63α was assessed at multiple time points in ovaries treated with CDDP at 4 μM (Figure 1cii). In order to expose PFs to damaging levels of CDDP in a shorter period, CDDP was also used at 10 (Figure 1ciii), 20, and 100 μM CDDP (Figure S1b and S1c). The effect of CDDP on the phosphorylation of TAp63α was dose-dependent: 10 μM CDDP shifted the major band of TAp63α similarly to X-ray-treated ovaries (Figure 1cii). Corresponding to the TAp63α phosphorylation patterns, the toxicity of 4 and 10 μM CDDP was qualitatively different: CDDP at 10 μM or higher severely damaged all cell types in the ovaries, whereas the toxicity of 4 μM CDDP was specific to PFs (Figure S1biv). Hence, the response of oocytes to 10 μM is irrelevant to the ovotoxicity of CDDP in cancer patients. Furthermore, imatinib and GNF-2 did not inhibit hyper-phosphorylation of TAp63α induced by X-ray (Figure 1civ), suggesting a fundamental difference between the signaling pathways activated by X-ray and 4 μM CDDP.

Although hyper-phosphorylation was undetectable in sodium dodecyl sulfate polyacrylamide gel electrophoresis (SDS-PAGE), 4 μM CDDP shifted the mobility of TAp63α in native PAGE (Fig. 1d), suggesting that tetramerization of TAp63α was induced by phosphorylation on a small number of critical residues.

The response of PFs to X-ray and 4 μM CDDP was further assessed by immunofluorescence (IF) assay. IF for cleaved-poly(ADP-ribose) polymerase (cPARP) indicated that apoptosis was activated in oocytes within a substantial portion of PFs by 6 and 24 h in X-irradiated and CDDP-treated ovaries, respectively (Fig. 1e). At these time points, DNA damage response (DDR) in oocytes of PFs was also at the peaked as assessed by γH2AX (Figure S2). The >3 kDa mobility shift of hyper-phosphorylated TAp63α suggested phosphorylation of additional residues to the known targets of CHEK2 and CK1. Accordingly, hyper-phosphorylation was assessed by phosphorylation of p63 on ser160/162 (p-p63). Indeed, almost all oocytes of PFs exhibited intense signals for p-p63 in X-irradiated ovaries at 6 h (Fig. 1e). In contrast, the majority of apoptotic oocytes in ovaries treated with 4 μM CDDP were negative for p-p63 at 24 h. The immunoblotting and IF data established that the phosphorylation patterns of TAp63α are distinctive between apoptosis of PFs induced by CDDP and IR.

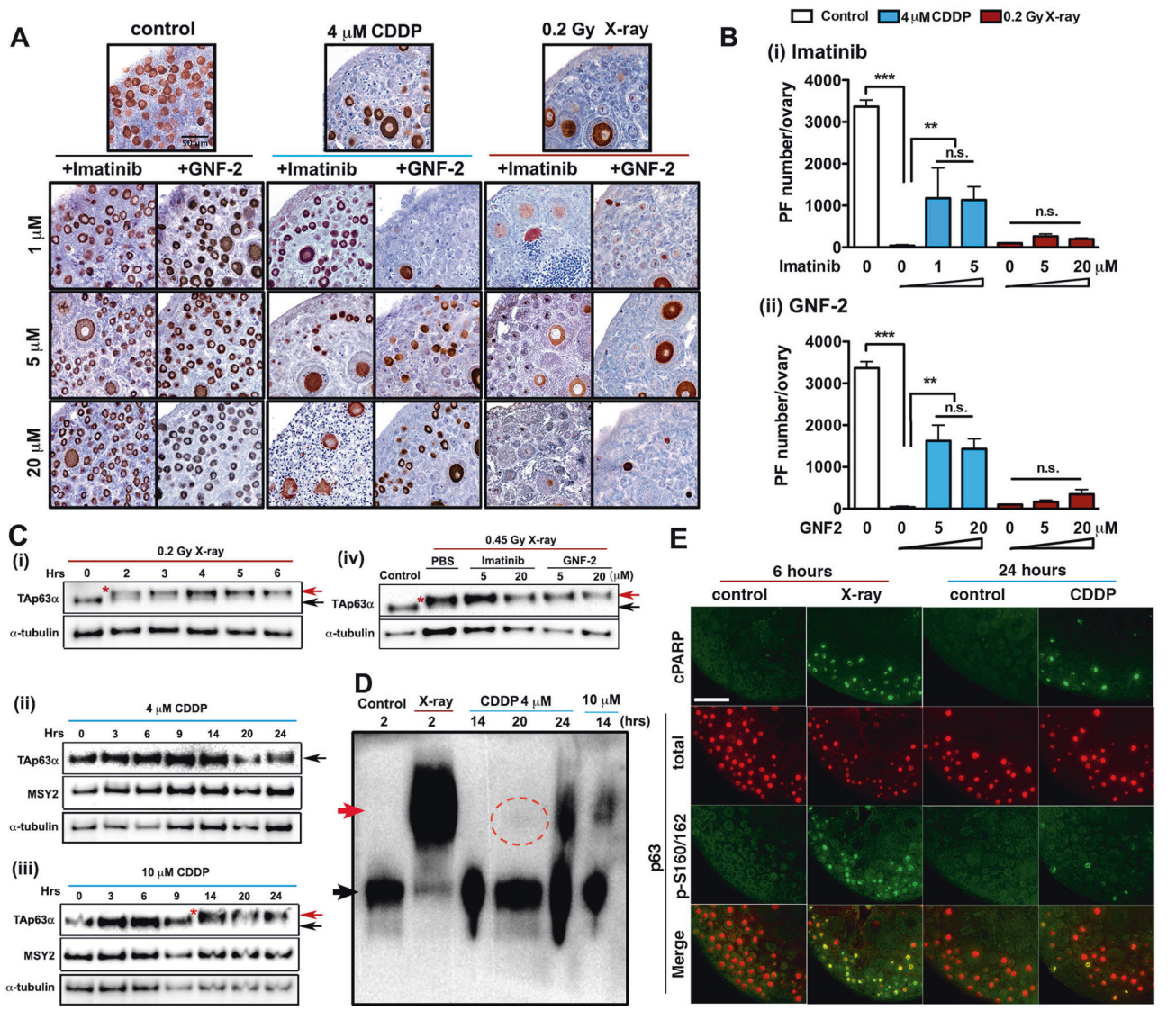

Fig. 1 CDDP and X-ray activate TAp63α through distinctive pathways. **a**, **b** Dose-dependent effect of imatinib and GNF-2 on the survival of PFs in organ culture assay. **a** MSY immunostaining. **b** The number of PFs per ovary ($n \geq 4$). **c** Mobility changes of TAp63α in X-irradiated and CDDP-exposed ovaries by SDS-PAGE. Time-course change by 0.2 Gy X-ray (i), 4 μM CDDP (ii), and 10 μM CDDP (iii). Effect of ABL inhibitors on the mobility of TAp63α by 0.45 Gy X-ray (iv). *, hyper-phosphorylated TAp63α. **d** Conformational change of TAp63α detected by native PAGE. The original and shifted positions of TAp63α are indicated by black and red arrows, respectively. The minor fraction of TAp63α shifted the mobility at 20 h after 4 μM CDDP-treatment (red dotted circle). **e** IF assay for cPARP and p-p63. Scale bar, 50 μm

Oocytic ABL kinases are dispensable for the activation of TAp63α

The distinctive phosphorylation patterns of TAp63α induced by CDDP and X-ray suggested the involvement of distinctive kinases in the activation of TAp63α. In fact, a previous study proposed that ABL1 activates TAp63α through phosphorylation of tyrosine residues in CDDP-damaged oocytes [5]. The protection of PFs from 4 μM CDDP by GNF-2, an allosteric ABL inhibitor, supported this model. Hence, we genetically tested the model in oocyte-specific conditional knockout (cKO) mice. At first, the essential role of TAp63α in both CDDP- and X-ray-induced apoptosis was confirmed in *Trp63* cKO mice: PFs of *Trp63* cKO *(Trp63$^{f/f}$;Gdf9-iCre)* mice were resistant to CDDP and X-ray (Fig. 2a). In contrast, oocyte-specific deletion of *Abl1 (Abl1$^{f/f}$;Gdf9-iCre)* did not protect PFs from CDDP or X-ray (Fig. 2b), despite efficient ablation of ABL1 from oocytes (Figure S3a). The ABL1 paralog ABL2/ARG was also expressed in the cytoplasm of oocytes within PFs (Figure S3a). Nonetheless, ovaries of *Abl2* cKO *(Abl2$^{f/f}$;Gdf9-iCre)* mice also lost PFs in response to CDDP (Fig. 2c). We further addressed the functional redundancy between ABL1 and

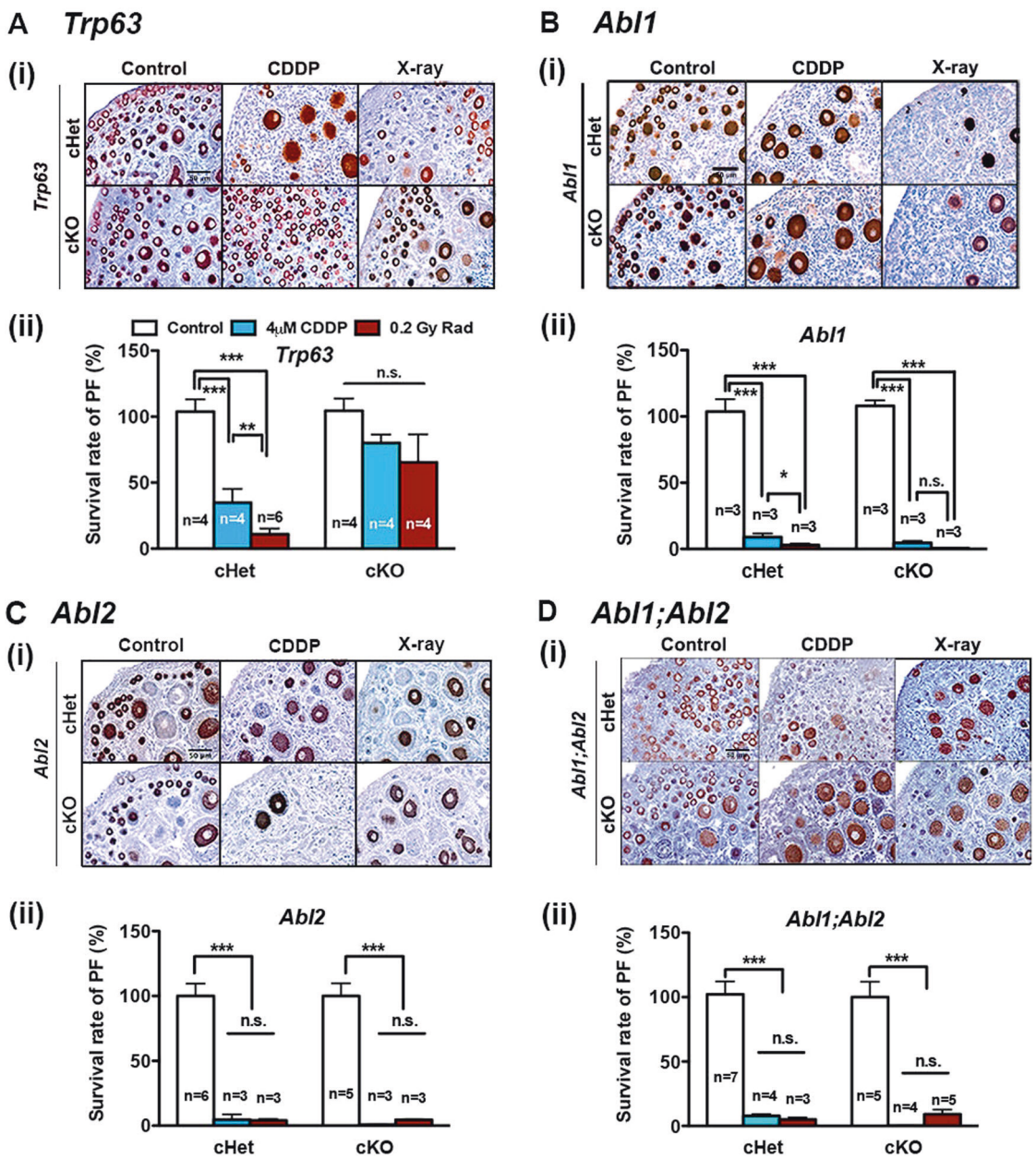

Fig. 2 Oocytic ABL kinases are dispensable for the activation of TAp63α. Ovaries from PD5 oocyte-specific conditional heterozygous (cHet) and cKO mice for *Trp63* (**a**), *Abl1* (**b**), *Abl2* (**c**), and *Abl1*;*Abl2* (**d**) were exposed to 4 μM CDDP or 0.2 Gy X-ray. The sample number (n) is marked on the bars. (i) MSY2 immunostaining ($n \geq 3$) (ii) survival rates of PFs (%) were normalized to the average PF number of the control group in each genotype

ABL2 in oocyte-specific double cKO mice of *Abl1* and *Abl2* (*Abl1*$^{f/f}$;*Abl2*$^{f/f}$;*Gdf9-iCre*). Unexpectedly, PFs of *Abl1*;*Abl2* cKO mice also underwent apoptosis in response to CDDP (Fig. 2d). Thus, ABL1 and ABL2 within oocytes are dispensable for CDDP-induced oocyte apoptosis, and the oocytic ABL kinases are not the target of GNF-2 in the protection of the ovarian reserve from CDDP. Finally, in agreement with inhibitor studies, X-ray induced hyper-phosphorylation of TAp63α in the ovaries of cKO mice for *Abl1* and/or *Abl2* (Fig. S3b), once again confirming that ABL kinases are dispensable for the hyper-phosphorylation of TAp63α.

CDDP and X-ray preferentially activate ATR and ATM, respectively

In general, DNA-adducts and DDSBs preferentially activate Ataxia Telangiectasia and Rad3-related (ATR) and Ataxia telangiectasia mutated (ATM), respectively. Accordingly, the efficacies of ATR and ATM inhibitors against CDDP

and X-ray were screened using ovarian organ culture. Dactolisib/NVP-BEZ235 (BEZ), an ATR inhibitor with moderate inhibitory activity against ATM [32], protected PFs from both CDDP and X-ray (Fig. 3a, b). Meanwhile, ETP-46464 (ETP) and AZD6738 (AZD), highly specific ATR inhibitors, effectively protected PFs from CDDP but the protection against X-ray was minimal (Fig. 3a, b). Conversely, KU-55933 (KU) [33], a highly specific inhibitor of ATM, protected PFs from X-ray [23], but not CDDP (Fig. 3a, b). The near-exclusive efficacies of ETP/AZD versus KU indicate that DDRs in oocytes for CDDP versus X-ray preferentially activate distinctive signaling pathways leading to apoptosis. Correspondingly, KU and BEZ, but not ETP and AZD, inhibited the hyper-phosphorylation of TAp63α induced by X-ray (Fig. 3c). Furthermore, CDDP preferentially induced phosphorylation of ATR over ATM, whereas X-ray preferentially induced phospho (p)-ATM over p-ATR in oocytes of PFs (Fig. 3d). Thus, CDDP and X-ray induce apoptosis in oocytes primarily through activation of ATR and ATM, respectively.

It has been proposed that DNA damage promotes transformation of PFs to primary follicles via activation of phosphatidylinositol-4,5-bisphosphate 3-kinase (PI3K) > AKT > mTORC1 pathway, thereby depleting the ovarian reserve [4, 10, 34]. As BEZ is an inhibitor of PI3K and mTOR [35], we tested if inhibition of the PI3K/mTORC1 pathway could protect PFs from CDDP and X-ray independent of ATM/ATR inhibition. However, three specific

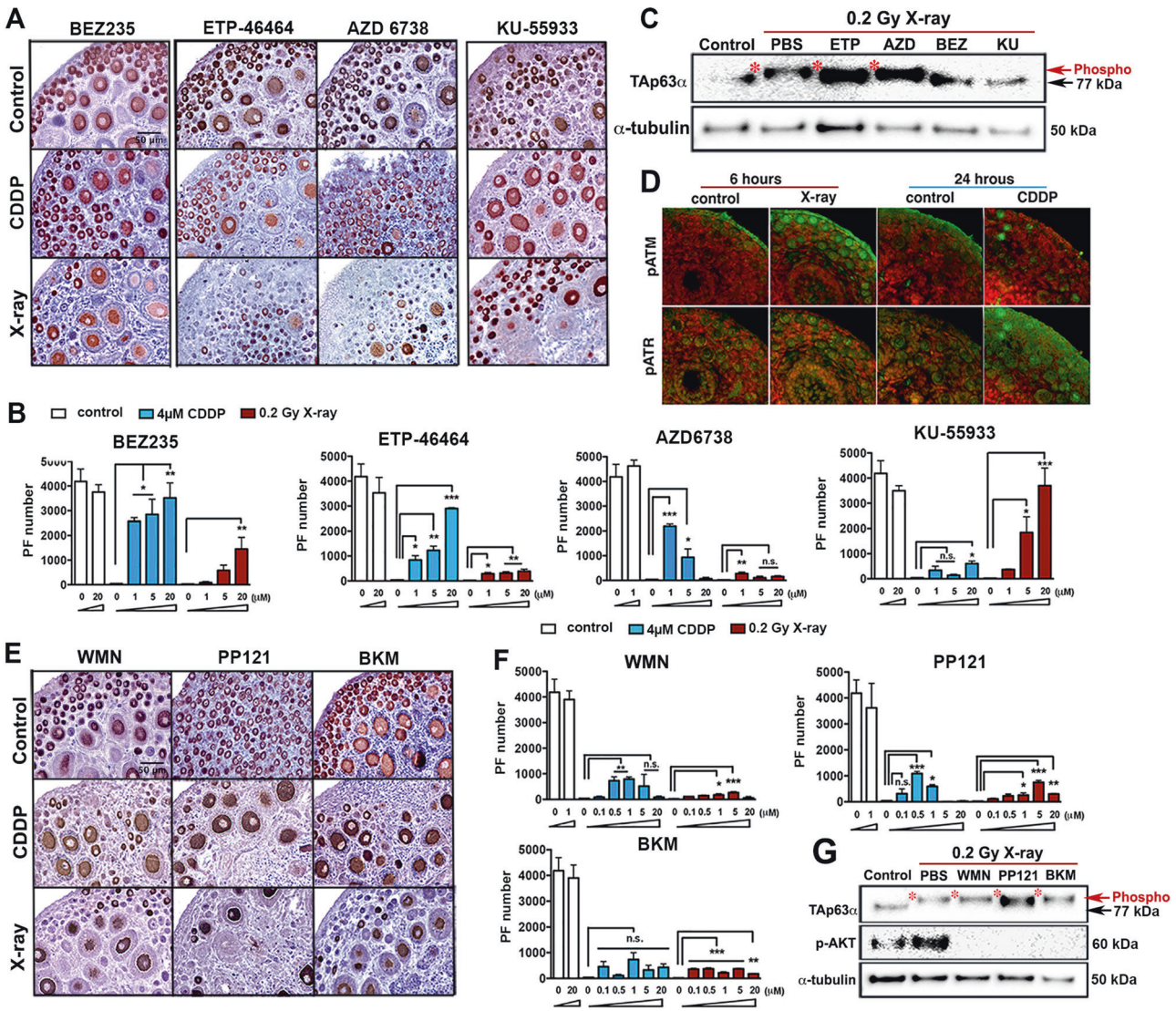

Fig. 3 CDDP and X-ray preferentially activate ATR and ATM, respectively. MSY immunostaining ($n \geq 3$) **a** and PF number **b** in ovaries treated with ATM/ATR inhibitors and CDDP or X-ray ($n = 3$). **a** Histology of ovaries with most effective dose of inhibitors. **c** Effect of ATM/ATR inhibitors on hyper-phosphorylation of TAp63α ($n = 3$). **d** IF assay for p-ATM and p-ATR. Red: DNA counterstaining. **e**, **f** MSY immunostaining **e** and PF number ($n = 3$) **f** in ovaries treated with CDDP/X-ray and Wortmannin (WMN), PP121, or BKM120 (BMK) ($n = 3$). **g** Effect of PI3K/mTOR inhibitors on p-AKT and hyper-phosphorylation of TAp63α ($n = 3$)

inhibitors of PI3K/mTORC1: Wortmannin, PP121, and BKM120, did not show comparable efficacy to ATM/ATR inhibitors in the protection of PFs from either CDDP or X-ray (Fig. 3e, f), even though phosphorylation of AKT was effectively repressed (Fig. 3g). A weak protective effect on PFs (~ 10–20%) by these PI3K/mTORC1 inhibitors likely occurred through their known inhibitory actions against ATM/ATR and ABL1/ABL2. Thus, we conclude that inhibition of PI3K > AKT > mTOR pathway does not protect PFs from CDDP or X-ray.

CDDP and X-ray preferentially activate CHEK1 and CHEK2, respectively

IR did not induce oocyte apoptosis and TAp63α-hyper-phosphorylation in *Chek2* null mice [24], suggesting that damage by IR is transduced through DDSB > ATM > CHEK2 > TAp63α-hyper-phosphorylation pathway. This model was further confirmed by Tuppi et al.: KU blocked the tetramerization of TAp63α induced by X-ray [23]. Meanwhile, given CHEK1 as the canonical downstream kinase of ATR, CDDP should activate TAp63α primarily through the platinum-DNA-adduct > ATR > CHEK1 pathway. Indeed, strong signals for p-CHEK2 and p-CHEK1 were preferentially detected in the nucleus of oocytes in PFs exposed to X-ray and CDDP, respectively (Fig. 4a), and the upregulation of p-CHEK1 was detected with CDDP but not X-ray by immunoblotting assay (Fig. 4b). Furthermore, two CHEK1 inhibitors, CHIR-124 [36] and MK-8776 [37] protected ~80% of PFs from CDDP, whereas they were totally ineffective against X-ray (Fig. 4c). However, owing to their toxicity toward somatic cells, CHEK1 inhibitors had relatively narrow effective dose-ranges in ovarian reserve protection (Figure S4b). In contrast, Chk2 inhibitor II hydrate (CK2II), which preferentially inhibits CHEK2 over CHEK1 (IC50; CHEK2 = 15 nM, CHEK1 = 17 μM) attenuated apoptosis of PFs by ~ 50% in both CDDP-treated and X-irradiated ovaries (Fig. 4d and S4c). Correspondingly, CK2II but not CHEK1 inhibitors blocked the hyper-phosphorylation of TAp63α in X-irradiated ovaries (Fig. 4e). However, IF assay revealed that CK2II attenuated the phosphorylation of ATM as well as CHEK2 (Fig. 4f), raising an issue in its target specificity. In fact, CK2II showed an inhibitory effect against a broad spectrum of kinases, reducing p-CHEK1 as well as the overall DDRs including γH2AX and p-ATR in CDDP-treated ovaries (Fig. 4g). Thus, the previously reported protective effect of CK2II on PFs against IR was likely through the global repression of DDRs, not necessarily specific inhibition of CHEK2. Meanwhile, imatinib did not repress DDRs (Fig. 4g), indicating ABL inhibitors protect PFs from CDDP through a distinct mechanism from the inhibitors of the ATR > CHEK1 pathway.

TAp73α regulates CDDP-induced primordial follicle loss

As previously reported [18], TAp73α, the dominant isoform of p73 in the ovary, was upregulated in the oocytes of PFs with CDDP exposure (Figs. 4b and 5a, b). X-irradiated oocytes showed moderate upregulation of TAp73 (Fig. 5b), which was below the detection threshold of immunoblotting. A role for TAp73α in PF apoptosis was tested in *Trp73* cKO mice (Fig. 5c and Figure S5). In organ culture assay, the PFs in the ovaries of *Trp73* cKO mice were protected from CDDP by ~30% but not from X-ray (Fig. 5d, e). The minor but consistent protection of PFs from CDDP in *Trp73* cKO mice indicates TAp73α sensitizes PFs to CDDP-induced apoptosis.

CK2II preserves fertility in female mice exposed to CDDP and X-ray

The organ culture assay does not determine whether the follicles/oocytes can survive and function for a long time. Accordingly, the long-term efficacy of imatinib, GNF-2, and CK2II in protecting PFs from genotoxic agents was tested in a kidney-grafting assay (Figure S6a and S6b) [18]. Although imatinib showed a long-term protective effect on PFs against CDDP, GNF-2 showed no efficacy, likely owing to the reversible action and high inhibitory constant of GNF-2 against ABLs. Alternatively, the long-lasting effect of imatinib may be through inhibition of kinases other than ABLs. In agreement with in vitro study, imatinib was effective only against CDDP, whereas CK2II showed efficacy for PF protection against both CDDP and X-ray (Figure S6a to S6c).

In organ culture, the activity of inhibitors remains constant throughout the treatment. However, in vivo the activity of most inhibitors rapidly declines, as they are cleared from the system [38]. Therefore, results based on the assays in which ovaries are treated in vitro do not convey a practicable ovarian function-preserving therapy [25]. Hence, we tested the efficacy of CK2II for the preservation of ovarian functions against CDDP and X-ray in mice.

In the fertility test, female mice treated with 5 mg/kg CDDP lost 90% of PFs within a week (Fig. 6a), and stopped reproducing by 5 months after delivering 2–4 litters, ($n = 5$, Fig. 6b). In striking contrast, the fertility of female mice that received CDDP + CK2II was indistinguishable from that of control and CK2II-treated mice. There was no significant difference in litter size, parity number and cumulative pup number between control, CK2II, and CDDP + CK2II groups, but all these parameters were significantly reduced in the CDDP group (Fig. 6c). In addition, female mice from the CDDP + CK2II group maintained a significantly higher

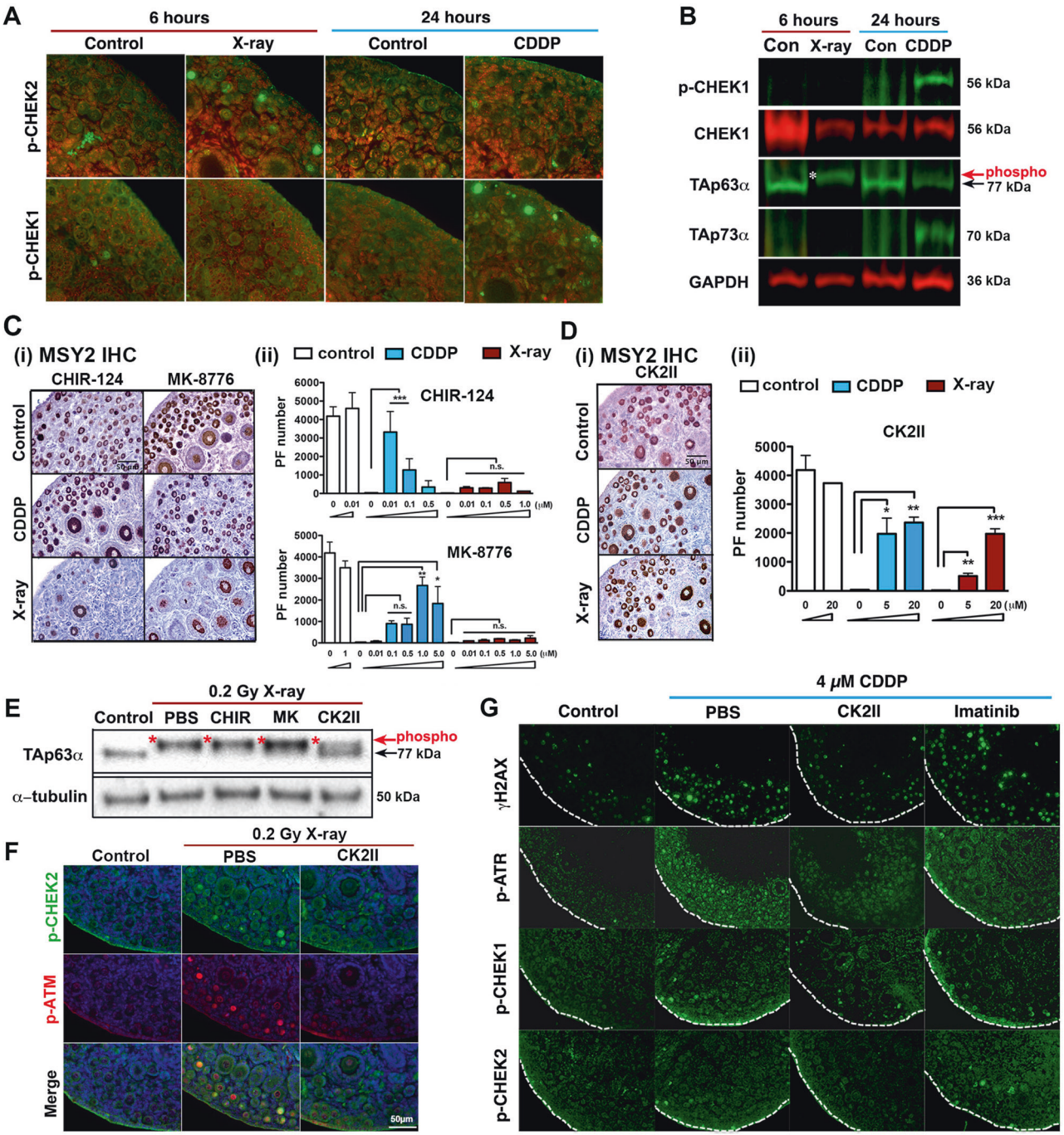

Fig. 4 X-ray and CDDP preferentially activate CHEK1 and CHEK2, respectively. **a** IF assay for p-CHEK2/p-CHEK1 (Green). Red: DNA counterstaining. **b** Immunoblotting analysis on p-CHEK1, CHEK1, TAp63α, and TAp73α in ovaries exposed to 0.2 Gy X-ray or 4 μM CDDP ($n \geq 3$). **c**, **d** MSY2 immunostaining (i) and PF number (ii) in the ovaries treated with CDDP/X-ray and CHEK1 inhibitors (**c**) or CHEK1/2 inhibitor **d** ($n = 3$). **e** Effect of CHEK1 and CHEK1/2 inhibitors on hyper-phosphorylation of TAp63α ($n = 3$). **f** Effect of CK2II on the X-ray-induced p-CHEK2 and p-ATM. **g** Effect of CK2II and imatinib on the CDDP-induced DDRs. White dotted lines outline the ovarian surface ($n = 3$)

number of PFs compared with the CDDP group (Figure 6civ). In fact, ovarian histology at 9 months was indistinguishable among control, CK2II and CDDP + CK2II groups (Fig. 6d), whereas the ovaries of the CDDP group contained small follicle-like structures devoid of oocytes (Fig. 6d, green arrow).

Based on the dose–response study (Figure S7), whole-body exposure to 0.1 Gy X-ray was used for the fertility test, as this dose reduced the PF number by 80% within a week (Figure 6ei). All X-irradiated female mice delivered up to 9 litters but lost fertility within 7 months ($n = 4$), whereas all X-ray + CK2II-treated female mice generated >

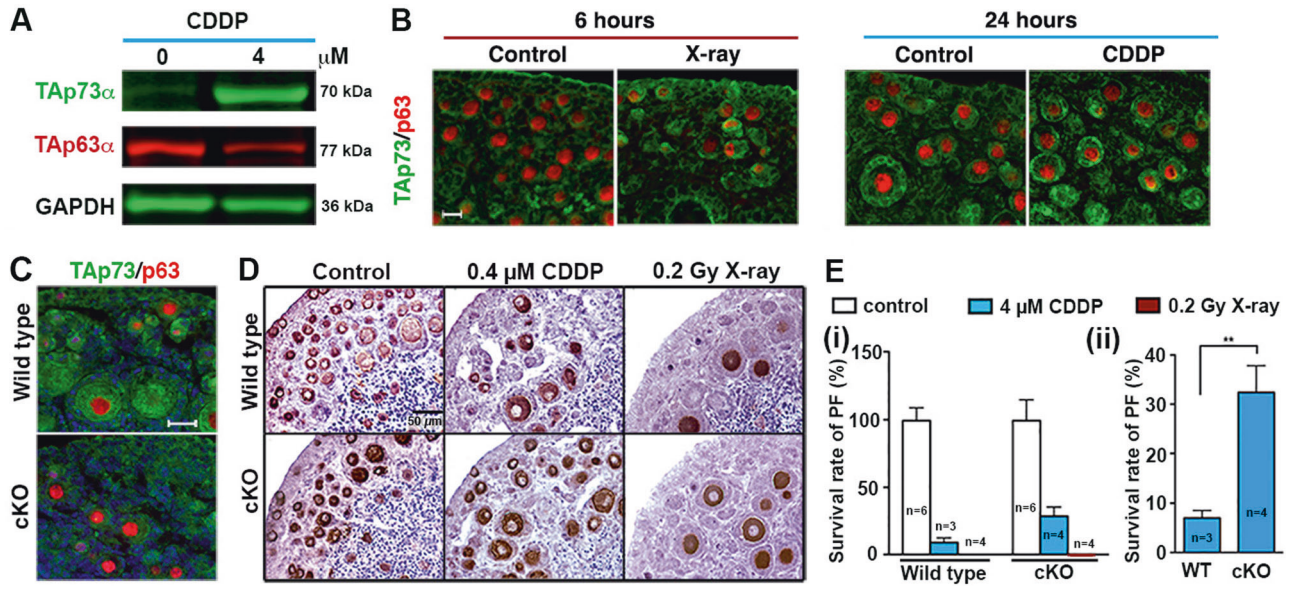

Fig. 5 TAp73α regulates CDDP-induced primordial follicle loss. Induction of TAp73α in PD5 mouse ovaries treated with 4 μM CDDP or 0.2 Gy X-ray **a** immunoblot (at 48 h) and **b** IF (at 24 h) TAp73 (green) and p63 (red). **c** IF assays of TAp73 (green) and p63 (red) (at 48 h). **d** MSY2 immunostaining (**e**) PF survival rate of Trp73 cKO (i) normalized to control and (ii) compared between wild type and cKO. The sample number (*n*) is marked on the bars

10 litters and remained fertile throughout the 9-month fertility test period (Figure 6eii). At the end of the fertility test, the ovaries from X-ray + CK2II female mice were heavier, containing a significantly higher number of PFs compared with the ovaries from X-irradiated females (Figure 6eiii, 6eiv and 6f).

Discussion

Our study establishes that X-ray and CDDP induce apoptosis in PFs by activating TAp63α primarily through different pathways (Fig. 7). Nonetheless, the transient repression of DDR protects the fertility of female mice from both CDDP and X-ray, establishing the feasibility of adjuvant therapies to protect ovarian functions against genotoxic therapies. Our data expand the previous model by elucidating the essential role of CHEK1 in determining the fate of CDDP-damaged oocytes. A paper, published while this manuscript was under the review, identified CK1 as an essential kinase that activate TAp63α in response to IR and 10 μM CDDP. In our current study, the requirement of CK1 for the PF-specific toxicity of CDDP remains unclear. However, it is possible that CDDP activates TAp63α via phosphorylation of a small number of residues by CHEK1 and CK1, as such a small molecular size change may not be detected by SDS-PAGE.

As a transient inhibition of DDR with non-toxic dose of an inhibitor is sufficient to protect the ovarian reserve, the feasibility of adjuvant therapy to protect PFs with CHEK1/2 inhibitors is founded. Generally, DNA lesions caused by genotoxic agents are not uniform, and both CDDP and IR can cause double-strand and single-strand breaks in genomic DNA. Thus, the dual inhibition of CHEK1 and CHEK2 seems to be critical to achieve a high efficacy of adjuvant therapies for ovarian reserve preservation. In this regard, several CHEK1/2 inhibitors (LY2606368, MK-8776, LY2603618, UCN-01) have already been used in clinical trials as anticancer therapeutics [39–42]. A caveat is that CK2II inhibits other DDR kinases than CHEK1/2, and the same efficacy may not be achieved with specific inhibitors of CHEK1/2.

There have been many other compounds shown to protect ovarian functions from genotoxic agents with diverse theories put forth for their mechanisms. For instance, it has been proposed that gonadotoxic agents deprive the ovarian reserve through spontaneous activation of PFs [4, 10, 34]. However, this theory is solely based on the systemic effects of inhibitors, the effect of which are not exclusive to the intended targets as shown herein. Our study clearly demonstrated that the activation of premature PFs is not the primary cause of ovarian failure induced by CDDP and IR. Nevertheless, other genotoxic agents such as cyclophosphamide may deplete the ovarian reserve through the activation of PFs. It should be noted that a recent genetic study demonstrated that mTORC1 activity is dispensable for the activation of PFs [43]. Accordingly, the systemic treatments with mTORC1 inhibitors may have protected the ovarian reserve from genotoxic agents by targeting other tissues/cells than oocytes. Elucidating the mode of action of

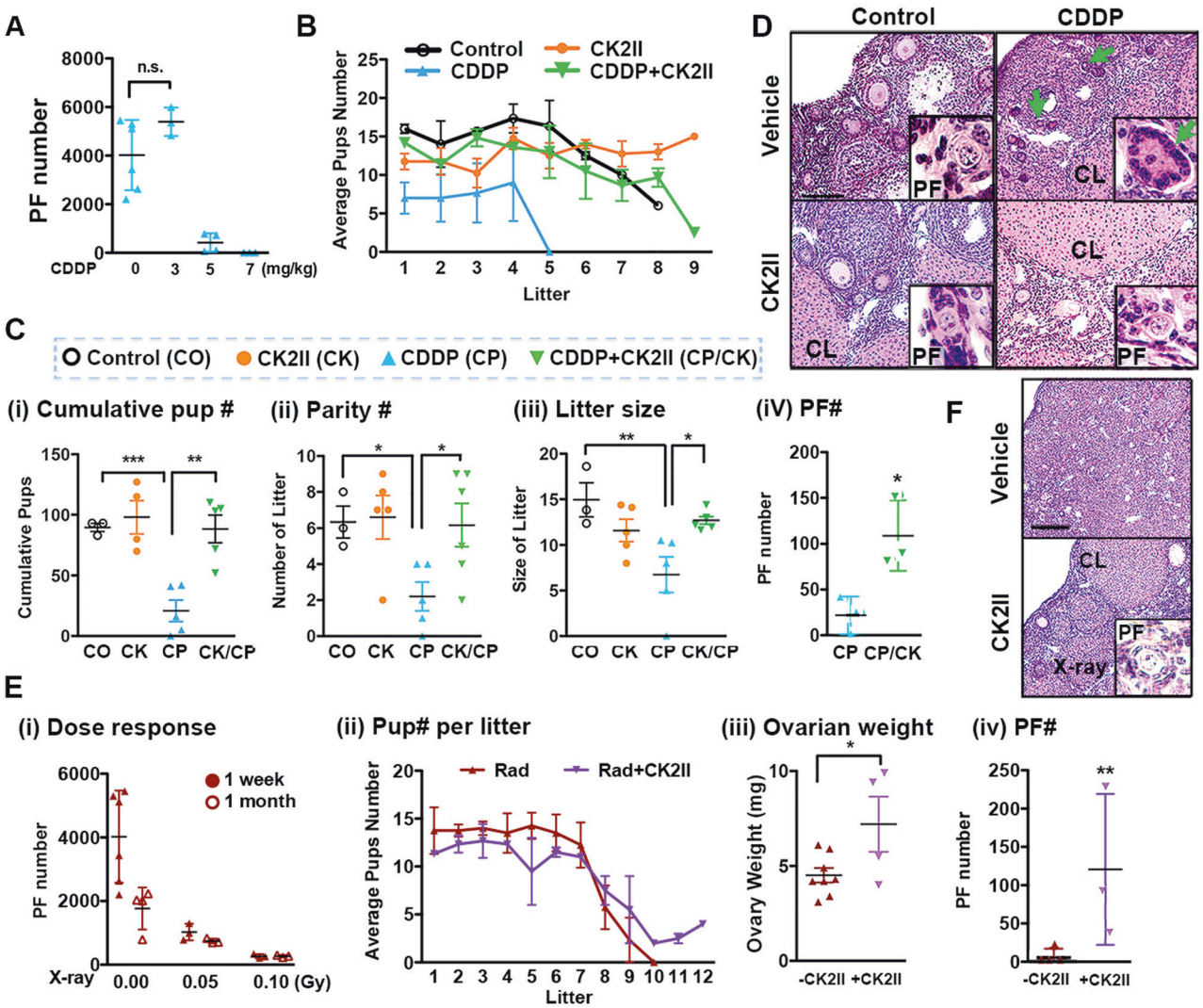

Fig. 6 CK2II preserves fertility in female mice exposed to CDDP and X-ray. **a** CDDP dose-effect on PF number per ovary at 7-day post treatment ($n \geq 4$). **b** Time-course change in litter size of CDDP/CK2II-treated female mice. **c** Effect of CDDP and/or CK2II demonstrated by (i) cumulative pup number, (ii) parity number, (iii) litter size, and (iv) PF number per female at the end of 9 months fertility test. CO = control, CK = CK2II, CP = CDDP, CK/CP = CK2II + CDDP. **d** Ovarian histology after fertility test. PF, primordial follicle; PM, primary follicle; CL, corpus luteum. Green arrows, follicle-like structure devoid of oocytes. **e** Effect of X-ray and/or CK2II on fertility of female mice; X-ray dose-effect on PF number ($n \geq 4$) (i), time-course change in litter size (ii), ovarian weight at 11 months after X-irradiation (iii), and PF number 11 months after X-ray with or without CK2II (iv). **f** Ovarian histology of X-ray/CK2II-treated female mice at 11 months

mTORC1 inhibitors in ovarian reserve protection against cyclophosphamide both in vitro and in vivo will contribute greatly.

Our genetic study established that oocytic ABL1 as well as ABL2 are dispensable for the activation of TAp63α, revising a previously proposed model. Accordingly, the mechanisms through which imatinib and GNF-2 protect oocytes from CDDP remain unclear. There are two non-exclusive explanations: ABL kinase inhibitors protect PFs by targeting (1) somatic cells and (2) molecules other than ABL kinases. DDR signals can be rapidly transmitted to undamaged bystander cells [44], and CDDP damages somatic cells (Figure S3b), supporting the first theory. On the other hand, there is no known target of GNF-2 other than ABL kinases. These issues will be addressed in cell-type-specific cKO mouse studies.

TAp63α and p53 play critical role in damage-induced apoptosis of female germ cells. Our current study adds TAp73α to the list of p53 homologs that protect the genetic integrity of the germline. TAp73α has been shown to regulate apoptosis triggered by mitochondrial dysfunction [45]. Hence, the function of TAp73α may be to remove oocytes with non-genomic damage. In fact, the toxicity of CDDP originates from multiple sources, including modifications of

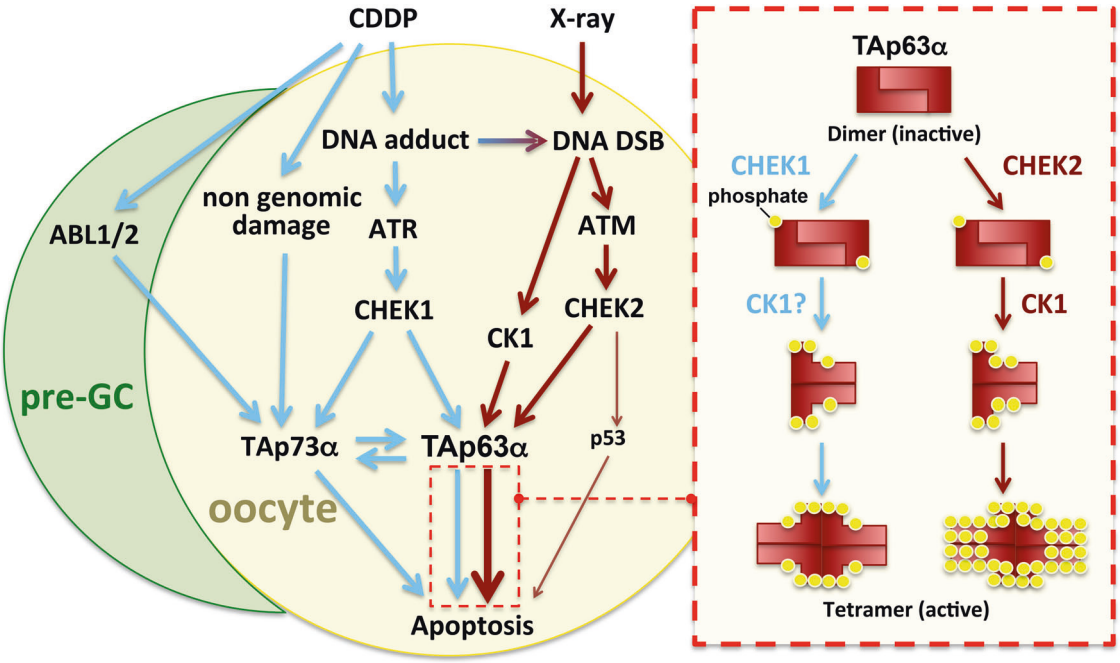

Fig. 7 Scheme of two distinct apoptotic pathways induced by X-ray and CDDP in primordial follicle. Light blue lines indicate apoptotic pathway induced by CDDP, whereas dark red lines induced by X-ray. The model for the conversion of TAp63α dimer to tetramer is shown in the box outlined by dotted lines. Yellow dots, phosphate; Pre-GC, pregranulosa cells

proteins, lipids and RNA [46]. The distinctive apoptotic signal transduction of CDDP versus X-ray in immature oocytes likely reflects the complexity of cellular damage caused by CDDP. Accordingly, the participation of three p53 homologs is critical for germ cell quality control, as they give oocytes the ability to die in response to different types of damage. Because fertility-preserving adjuvant therapies deceive this safeguard system, thereby allowing oocytes that were destined to die to persist, genomic integrity becomes a concerning issue [47]. Previous studies have concluded adjuvant therapies were safe, as no visible abnormalities were detected in pups born to female mice treated with genotoxic agents and adjuvants [4, 5, 7–9, 25]. However, the limitation of phenotype-based mutagenesis assay has been demonstrated by the ENU (N-ethyl-N-nitrosourea) mutagenesis in the mouse, which increases de novo single nucleotide variants in progenies by 133-fold (7.18×10^{-7} per nucleotide, 2105 de novo SVNs per generation) [48], resulting in ~25 mutations with functional consequences per diploid genome. However, even with such an extremely high mutation rate, most abnormalities do not appear in the first generation progeny because only 0.1–2% of such mutations generate dominant alleles [49]. In order to assess the risk of the adjuvant therapies, the genetic integrity of offspring must be quantitatively assessed by whole genome or exome sequencing. In humans, advanced paternal age is associated with an increase of point mutations in male germ cells: it has been estimated that 36-year-old men pass on twice more mutations to their children compared with 20-year-old men [50]. With this in mind, adjuvant therapies should be accepted if the increase in de novo mutation rate does not exceed the effect of natural aging. Even if the mutation rate is elevated in oocytes to a level that reproduction should be prohibited, these therapies should still be offered to maintain crucial ovarian endocrine support and improve the post-treatment quality of life for female patients who receive gonadotoxic therapies.

Experimental procedures

Animals

All procedures involving mice were approved by the IACUC at Northwestern University and The Ohio State University. Mice were provided with food and water ad libitum. CD-1 mice were purchased from Harlan Laboratories (Madison, WI), and C57BL/6J, NSG (NOD.Cg-*Prkdc*^{scid} *Il2rg*^{tm1Wjl}/SzJ) [51] and *Gdf9-iCre* mice were purchased from Jackson Laboratories (Bar Harbor, ME) [52]. Mice carrying a floxed allele for *Trp63*, *Abl1* (B6.129P2-*Abl1*$^{tm2.1Goff}$/J) [53] were previously described. Mice carrying a floxed allele for *Abl2* were generated as described in Figure S8. Mice carrying a floxed allele for *Trp73* (*Trp73*^{flox}) were generated from ES cells carrying the *Trp73*$^{tm1a(KOMP)Wtsi}$ allele (CSD89710, KOMP) at Transgenic and Targeted Mutagenesis Laboratory (TTML) (Northwestern Feinberg School of Medicine). The

LacZ-Neo cassette was then removed by crossing *Trp73*$^{tm1a(KOMP)Wtsi}$ mice to B6.Cg-Tg(ACTFLPe)9205Dym/J mice [54, 55].

Oocyte-specific cKO mice were generated by breeding female homozygous mice for the floxed allele with male heterozygous mice for the floxed allele and *Gdf9-iCre*. The genotyping PCR conditions (primer sequences, annealing temperature and product size) are as follows: *Abl1*, F, 5′-AGCCACTTCGGATTTAGTTGAA-3′, R, 5-GCAACC GGCTTGCATGT-3′, annealing at 60 °C, the products for floxed and wild-type alleles are 350 and 250 bp, respectively; *Abl2*, F, 5′-GCAGCCTTTGGCTTTATCGTCTAA GGG-3′, R, 5′-GCCATCCTGGTGTGGTGATGTTTAC-3′, annealing at 67 °C, the products for floxed and wild-type alleles are 400 and 270 bp, respectively; *Trp73*, F, 5′- CAACAGCTTGGCTGCCTGGACTTGG-3′, R, 5′-CA GTCCTAGTTTTGCTTTCCCAGCC-3′, two-step annealing with 65 °C for 15 s and 55 °C for 30 s, the products for floxed and wild-type alleles are 475 and 269 bp, respectively. For all reactions, 94 and 72 °C were used for denaturation and extension, respectively. The genotyping protocols for *Gdf9-iCre* and *Trp63* have been described previously [18].

Whole-ovary organ culture

Ovarian organ culture was performed as previously described [18]. In brief, ovaries collected from postnatal day 5 (PD5, the day of birth as PD0) mice were cultured at 37 °C under 5% CO_2 in a medium containing an inhibitor or vehicle only (control) for 2 h prior to the treatment with 4 μM CDDP (P4394, MilliporeSigma, St. Louis, MO) or 0.2 Gy X-ray (RS-2000×-Ray Irradiator (Rad Source Technologies, Buford, GA)). The medium was changed at 48 h, and the inhibitors were maintained in the culture medium at the same concentration throughout the treatment. The number of PFs was determined at 48 h for X-ray and 96 h for CDDP because apoptosis occurred within this time frame, and the number of survived PFs did not change even when ovaries were cultured for an extended period. PF numbers in control groups were identical at 48, 72, and 96 h. Hence, the control groups for CDDP and X-ray were combined to calculate the average PF number, which was used as 100% survival. Although the center of cultured ovaries often exhibited necrosis owing to hypoxia, it did not compromise the analyses, as necrosis within 5 days occurred far from the periphery where PFs reside. For cKO studies, ovaries from a single mouse were always used in a paired fashion: control and CDDP or control and X-ray treated groups. Therefore, the PF number of CDDP/X-ray treated samples was expressed as the ratio to the PF number in the paired control ovary. The S.D. for the control group was calculated with the PF numbers of control ovaries converted into a percent of their average. For the subrenal grafting assay, ovaries were cultured for 24 h in vitro and then transplanted into the NSG mice.

The dose of CDDP in organ culture was based on the plasma concentration of CDDP in patients receiving CDDP-chemotherapy: the plasma CDDP concentration of patients who received 30-min daily infusions of CDDP for 3 days was maintained between 1.5 and 6 μM [31]. We used 0.2 Gy X-irradiation for the organ culture assay because it specifically destroyed > 90% of PFs within 24 h without damaging secondary follicles and somatic cells (Figure S1d). For IF and immunoblotting assays, 6 h for X-irradiation and 24 h for CDDP-treatment were used, based upon time-course analysis for γH2AX and cPARP (Figure S2). However, higher doses of CDDP (10, 20 and 100 μM) and X-ray (0.45 Gy) were also used for the sensitive detection of TAp63α hyper-phosphorylation as indicated. CDDP was freshly prepared with Dulbecco's phosphate-buffered saline (DPBS) (Ca^{2+} free and Mg^{2+} free) within 30 min prior to the experiment. The catalog number and source of chemicals were as follows: Imatinib (5906, R&D Systems, Minneapolis, MN), Nilotinib (Reagents direct, Encinitas, CA), GNF-2 (G9420), Wortmannin (W1628) and Chk2 inhibitor II hydrate (C3742) from MilliporeSigma; Dasatinib (S1021), ETP-46464 (S8050), AZD6738 (S7693), BEZ235 (S1009), BKM120 (S2247), CHIR-124 (S2683), and MK-8776 (S2735) from Selleck Chemicals, Houston, TX; KU-55933 (3544) and PP121 (3894) from Tocris Bioscience, Bristol, UK.

Subrenal grafting assay

Subrenal grafting assay was performed as previously described with minor modifications [18]. In brief, ovaries cultured with an inhibitor were rinsed twice with DPBS. Two ovaries per kidney were transplanted under the subrenal capsule of ovariectomized NSG mice (5–6 weeks of age). Both ovaries of the host were removed at the time of kidney grafting. Transplants were collected 30 days after grafting to determine the number of PFs per graft.

Follicle counting

Mouse ovaries were fixed with Modified Davison's fixative (64133-50, Electron Microscopy Science Inc., Hatfield, PA) for 24 h at 4 °C, processed into paraffin blocks and were entirely sectioned at 5 μm thickness. PFs were counted in every 10th section stained with Haemotoxylin and Eosin [56]. In order to determine the PF number per ovary, the average number of PFs per section was multiplied by the total number of sections and divided by the average number of sections in which a single PF appears. Because the last parameter is difficult to determine, we adapted the standard

formula used in previous studies for convenience to calculate the PF number per ovary: average PF number per section × total section number × ½ [56]. The PF number in graphs indicates total number of PFs per ovary. Though this number does not represent the actual PF number per ovary, the comparison of relative PF number between groups is still valid.

IF and immunohistochemistry (IHC)

The details have been described previously [57]. Primary antibodies against phospho-p63 (Ser160/162) (#4981, 1:50), phospho-ATR (Ser428) (#2853, 1:150), phospho-ATM (Ser1981) (#4526, 1:200), phospho-CHEK1 (Ser317) (#12302, 1:200), phospho-CHEK2 (Thr68) (#2197, 1:100), cleaved-PARP (#9544, 1:50) and phospho-Histone H2A.X (Ser139, γH2AX) (#9718, 1:500) were purchased from Cell Signaling Technology (Danvers, MA); p63 (4A4) (CM163A, 1:500) was purchased from BioCare Medical (Pacheco, CA); TAp73 (IHC-00197, 1:200) was purchased from Bethyl Laboratories (Montgomery, TX); and MSY2 (1: 4000) was a gift from Dr. Schultz RM, University of Pennsylvania. For IF, AlexaFluor594-anti-mouse IgG (715-586-150, 1:1000) and AlexaFluor488-anti-rabbit IgG (711-546-152, 1:1000) from Jackson ImmunoResearch (West Grove, PA) were used for the secondary antibodies, and bisbenzimide H 33258 (14530, 1:10,000) from MilliporeSigma was used for nuclear staining. For IHC, the DAB Peroxidase Substrate Kit (SK-4100, Vector Laboratories, Burlingame, CA) was used.

Immunoblot analysis

PD5 mouse ovaries were homogenized with a minipestle in ice-cold lysis buffer containing protease (4693159001, Roche, Basel, Switzerland) and phosphatase (4906845001, Roche) inhibitors and loaded into Bis-Tris precast SDS-PAGE gel with NuPAGE 4–12% gradient. Proteins were transferred to a nitrocellulose/PVDF membrane. For detecting phosphorylation of TAp63α, SDS-PAGE gel was run for 4 h and 30 min at 150 V. Primary antibodies used for immunoblotting were as follows: phospho-p63 Ser160/162 (#4981), p63α (#4892), p-AKT (#9271), PARP (#9542) and p-CHEK1 (#12302) from Cell Signaling Technology: α-tubulin (T9026) and GAPDH (G8795) from MilliporeSigma: p63 (4A4) (790-4509, Ventana Medical Systems, Tucson, AZ), CHEK1 (G-4) (sc-8408, Santa Cruz Biotechnology, Santa Cruz, CA) and TAp73 (A300-126A, Bethyl Laboratories, Montgomery, TX). ECL Prime (89168-782, GE Healthcare Biosciences, Pittsburgh, PA) and Luminata Crescendo Western HRP substrate (WBLUR0500, EMD Millipore, Germany) were used for immunoblotted protein detection by The FluorChem HD Imaging System (Alpha Innotech Co, Gauteng, South Africa), Azure c500 (Azure Biosystems, Inc., Dublin, CA) and Odyssey CLx Imaging System (LI-COR Biosciences, Lincoln, NE). To test other antibodies, membranes were stripped by using Restore™ western blot Stripping Buffer (21059, ThermoFisher Scientific, Waltham, MA) and reused. α-tubulin or GAPDH were used for loading control.

Blue native PAGE

For blue native PAGE (BN-PAGE) analysis of the tetramerization state of TAp63α, four ovaries were used for each group at the indicated condition. The ovaries were lysed in sample buffer, supplemented with 1 × protease (4693159001, Roche) and phosphatase (4906845001, Roche) inhibitors. The supernatant was loaded into a BN-PAGE Novex 3–12% Bis-Tris protein gel system (BN1001BOX, Thermofisher Scientific) according to the manufacturer's instructions. The cathode buffer was supplemented with Coomassie G250 (BN2004, Thermofisher Scientific) and the gel was run at 4 °C for 30 min at 150 V, then 1 h at 250 V. Proteins were transferred to a Invitrolon™ PVDF/Filter Paper Sandwich membrane (LC2005, Thermofisher Scientific).

Fertility test

CK2II injection-solution was prepared with 8:2 mixture of dimethyl sulfoxide (D8418, MilliporeSigma) and DPBS at 0.8 mg/ml. CK2II (1.0 mg/Kg BW), or vehicle was injected intraperitoneally into PD5 female CD-1 mice using a Hamilton Syringe (7637-01, Hamilton Company, Reno, NV) with a 33-gauge needle (7803-05, Hamilton Company) 2 h prior to treatment with 0.1 Gy X-ray or 5 mg/kg CDDP (equivalent to 15 mg/m^2 body surface area in human patients) [58]. At PD35, treated female mice were subjected to fertility testing with mature male CD-1 mice (7–8 weeks old) by continuous trio breeding. The reproductive activity of female mice (parity number and litter size) was monitored for 9 months for CDDP experiment (vehicle control, CDDP, CK2II, CDDP + CK2II) and 11 months for X-ray experiment (X-ray and X-ray + CK2II). When female mice delivered, the litter remained with the mother for 5 days and then was euthanized. The fertility test was stopped when pregnancy was not observed in all female mice of one treatment-group for 2 months, and the female mice were killed to collect ovaries for analyses.

Statistics

Data are presented by means ± S.D. For a comparison of means between more than two independent groups, one-way analysis of variance was performed, whereas the difference between two groups was analyzed by Tukey's range test for

statistical comparisons using PRISM 5.0 (GraphPad Software). Values of $P < 0.05$ were considered to be statistically significant. Statistical significance was marked as ***, $P < 0.001$; **, $P < 0.01$; *, $P < 0.05$; n.s., non-significant.

Acknowledgements We thank the Center for Reproductive Health After Disease (P50HD076188) from the National Institutes of Health National Center for Translational Research in Reproduction and Infertility (NCTRI) (to SYK, DMN, MR, VAS, and TK), the Comprehensive Cancer Center, The Ohio State University (to DMN, VAS, and TK), Grants P30CA016058, R01CA154358, and R01HD064402 (to DMN, VAS, and TK) and R01NS089662 (to AJK). We thank Pavithra Kannan, Shayna Wallace, and Justin Thomas at OSU for genotyping and imaging and Keisha M. Barreto at NU for sectioning ovarian samples.

Author contributions SYK and TK designed the study; SYK, DMN, MR, VAS, and TK performed experiments; SYK, DMN, and TK collected and analyzed data; TKW provided conceptual advice; AJK provided *Abl2* floxed mice; SYK and TK wrote the manuscript; SYK, DMN, MR, VAS, AJK, TKW, and TK edited the manuscript.

Compliance with ethical standards

Conflict of interest The authors declare that they have no conflict of interest.

References

1. Pacheco A, Cruz M, Garcia Velasco JA. Impact of very low anti-Mullerian hormone on pregnancy success. Curr Opin Obstet Gynecol. 2017;29:131–5.
2. Donfack NJ, Alves KA, Araujo VR, Cordova A, Figueiredo JR, Smitz J, et al. Expectations and limitations of ovarian tissue transplantation. Zygote. 2017;25:391–403.
3. Jensen AK, Kristensen SG, Macklon KT, Jeppesen JV, Fedder J, Ernst E, et al. Outcomes of transplantations of cryopreserved ovarian tissue to 41 women in Denmark. Hum Reprod. 2015;30:2838–45.
4. Kalich-Philosoph L, Roness H, Carmely A, Fishel-Bartal M, Ligumsky H, Paglin S, et al. Cyclophosphamide triggers follicle activation and "burnout"; AS101 prevents follicle loss and preserves fertility. Sci Transl Med. 2013;5:185ra62.
5. Gonfloni S, Di Tella L, Caldarola S, Cannata SM, Klinger FG, Di Bartolomeo C, et al. Inhibition of the c-Abl-TAp63 pathway protects mouse oocytes from chemotherapy-induced death. Nat Med. 2009;15:1179–85.
6. Piasecka-Srader J, Blanco FF, Delman DH, Dixon DA, Geiser JL, Ciereszko RE, et al. Tamoxifen prevents apoptosis and follicle loss from cyclophosphamide in cultured rat ovaries. Biol Reprod. 2015;92:132.
7. Rossi V, Lispi M, Longobardi S, Mattei M, Rella FD, Salustri A, et al. LH prevents cisplatin-induced apoptosis in oocytes and preserves female fertility in mouse. Cell Death Differ. 2017;24:72–82.
8. Zelinski MB, Murphy MK, Lawson MS, Jurisicova A, Pau KY, Toscano NP, et al. In vivo delivery of FTY720 prevents radiation-induced ovarian failure and infertility in adult female nonhuman primates. Fertil Steril. 2011;95:1440-5 e1-7.
9. Kano M, Sosulski AE, Zhang L, Saatcioglu HD, Wang D, Nagykery N, et al. AMH/MIS as a contraceptive that protects the ovarian reserve during chemotherapy. Proc Natl Acad Sci USA. 2017;114:E1688–97.
10. Jang H, Lee OH, Lee Y, Yoon H, Chang EM, Park M, et al. Melatonin prevents cisplatin-induced primordial follicle loss via suppression of PTEN/AKT/FOXO3a pathway activation in the mouse ovary. J Pineal Res. 2016;60:336–47.
11. Coutandin D, Ou HD, Lohr F, Dotsch V. Tracing the protectors path from the germline to the genome. Proc Natl Acad Sci USA. 2010;107:15318–25.
12. Pankow S, Bamberger C. The p53 tumor suppressor-like protein nvp63 mediates selective germ cell death in the sea anemone Nematostella vectensis. PLoS ONE. 2007;2:e782.
13. Schumacher B, Hofmann K, Boulton S, Gartner A. The C. elegans homolog of the p53 tumor suppressor is required for DNA damage-induced apoptosis. Curr Biol. 2001;11:1722–7.
14. Derry WB, Putzke AP, Rothman JH. Caenorhabditis elegansp53: role in apoptosis, meiosis, and stress resistance. Science. 2001;294:591–5.
15. Amelio I, Grespi F, Annicchiarico-Petruzzelli M, Melino G. p63 the guardian of human reproduction. Cell Cycle. 2012;11:4545–51.
16. Dotsch V, Bernassola F, Coutandin D, Candi E, Melino G. p63 and p73, the ancestors of p53. Cold Spring Harb Perspect Biol. 2010;2:a004887.
17. Suh EK, Yang A, Kettenbach A, Bamberger C, Michaelis AH, Zhu Z, et al. p63 protects the female germ line during meiotic arrest. Nature. 2006;444:624–8.
18. Kim SY, Cordeiro MH, Serna VA, Ebbert K, Butler LM, Sinha S, et al. Rescue of platinum-damaged oocytes from programmed cell death through inactivation of the p53 family signaling network. Cell Death Differ. 2013;20:987–97.
19. Kurita T, Cunha GR, Robboy SJ, Mills AA, Medina RT. Differential expression of p63 isoforms in female reproductive organs. Mech Dev. 2005;122:1043–55.
20. Livera G, Petre-Lazar B, Guerquin MJ, Trautmann E, Coffigny H, Habert R. p63 null mutation protects mouse oocytes from radio-induced apoptosis. Reproduction. 2008;135:3–12.
21. Deutsch GB, Zielonka EM, Coutandin D, Weber TA, Schafer B, Hannewald J, et al. DNA damage in oocytes induces a switch of the quality control factor TAp63α from dimer to tetramer. Cell. 2011;144:566–76.
22. Deutsch GB, Zielonka EM, Coutandin D, Dotsch V. Quality control in oocytes: domain-domain interactions regulate the activity of p63. Cell Cycle. 2011;10:1884–5.
23. Coutandin D, Osterburg C, Srivastav RK, Sumyk M, Kehrloesser S, Gebel J, et al. Quality control in oocytes by p63 is based on a spring-loaded activation mechanism on the molecular and cellular level. eLife. 2016;5:pii: e13909.
24. Bolcun-Filas E, Rinaldi VD, White ME, Schimenti JC. Reversal of female infertility by Chk2 ablation reveals the oocyte DNA damage checkpoint pathway. Science. 2014;343:533–6.
25. Rinaldi VD, Hsieh K, Munroe R, Bolcun-Filas E, Schimenti JC. Pharmacological inhibition of the dna damage checkpoint prevents radiation-induced oocyte death. Genetics. 2017;206:1823–8.
26. Tuppi M, Kehrloesser S, Coutandin DW, Rossi V, Luh LM, Strubel A, et al. Oocyte DNA damage quality control requires consecutive interplay of CHK2 and CK1 to activate p63. Nat Struct Mol Biol. 2018;25:261–9.
27. Maiani E, Di Bartolomeo C, Klinger FG, Cannata SM, Bernardini S, Chateauvieux S, et al. Reply to: cisplatin-induced primordial follicle oocyte killing and loss of fertility are not prevented by imatinib. Nat Med. 2012;18:1172–4.
28. Kerr JB,Hutt KJ,Cook M,Speed TP,Strasser A,Findlay JK, et al. Cisplatin-induced primordial follicle oocyte killing and loss of fertility are not prevented by imatinib. Nat Med. 2012;18:1170–2.
29. Gonfloni S. DNA damage stress response in germ cells: role of c-Abl and clinical implications. Oncogene. 2010;29:6193–202.
30. Tomasini R, Tsuchihara K, Wilhelm M, Fujitani M, Rufini A, Cheung CC, et al. TAp73 knockout shows genomic instability

with infertility and tumor suppressor functions. Genes Dev. 2008;22:2677–91.
31. Urien S, Lokiec F. Population pharmacokinetics of total and unbound plasma cisplatin in adult patients. Br J Clin Pharmacol. 2004;57:756–63.
32. Toledo LI, Murga M, Zur R, Soria R, Rodriguez A, Martinez S, et al. A cell-based screen identifies ATR inhibitors with synthetic lethal properties for cancer-associated mutations. Nat Struct Mol Biol. 2011;18:721–7.
33. Hickson I, Zhao Y, Richardson CJ, Green SJ, Martin NM, Orr AI, et al. Identification and characterization of a novel and specific inhibitor of the ataxia-telangiectasia mutated kinase ATM. Cancer Res. 2004;64:9152–9.
34. Goldman KN, Chenette D, Arju R, Duncan FE, Keefe DL, Grifo JA, et al. mTORC1/2 inhibition preserves ovarian function and fertility during genotoxic chemotherapy. Proc Natl Acad Sci USA. 2017;114:3186–91.
35. Maira SM, Stauffer F, Brueggen J, Furet P, Schnell C, Fritsch C, et al. Identification and characterization of NVP-BEZ235, a new orally available dual phosphatidylinositol 3-kinase/mammalian target of rapamycin inhibitor with potent in vivo antitumor activity. Mol Cancer Ther. 2008;7:1851–63.
36. Tse AN,Rendahl KG,Sheikh T,Cheema H,Aardalen K,Embry M, et al. CHIR-124, a novel potent inhibitor of Chk1, potentiates the cytotoxicity of topoisomerase I poisons in vitro and in vivo. Clin Cancer Res. 2007;13:591–602.
37. Guzi TJ, Paruch K, Dwyer MP, Labroli M, Shanahan F, Davis N, et al. Targeting the replication checkpoint using SCH 900776, a potent and functionally selective CHK1 inhibitor identified via high content screening. Mol Cancer Ther. 2011;10:591–602.
38. Leveque D, Maloisel F. Clinical pharmacokinetics of imatinib mesylate. Vivo. 2005;19:77–84.
39. Daud AI, Ashworth MT, Strosberg J, Goldman JW, Mendelson D, Springett G, et al. Phase I dose-escalation trial of checkpoint kinase 1 inhibitor MK-8776 as monotherapy and in combination with gemcitabine in patients with advanced solid tumors. J Clin Oncol. 2015;33:1060–6.
40. Calvo E, Braiteh F, Von Hoff D, McWilliams R, Becerra C, Galsky MD, et al. Phase I study of CHK1 inhibitor LY2603618 in combination with gemcitabine in patients with solid tumors. Oncology. 2016;91:251–60.
41. Hotte SJ, Oza A, Winquist EW, Moore M, Chen EX, Brown S, et al. Phase I trial of UCN-01 in combination with topotecan in patients with advanced solid cancers: a Princess Margaret Hospital Phase II Consortium study. Ann Oncol. 2006;17:334–40.
42. Hong D, Infante J, Janku F, Jones S, Nguyen LM, Burris H, et al. Phase I study of LY2606368, a checkpoint kinase 1 inhibitor, in patients with advanced cancer. J Clin Oncol. 2016;34:1764–71.
43. Gorre N, Adhikari D, Lindkvist R, Brannstrom M, Liu K, Shen Y. mTORC1 Signaling in oocytes is dispensable for the survival of primordial follicles and for female fertility. PLoS ONE. 2014;9: e110491.
44. Malaquin N, Carrier-Leclerc A, Dessureault M, Rodier F. DDR-mediated crosstalk between DNA-damaged cells and their microenvironment. Front Genet. 2015;6:94.
45. Liu T, Roh SE, Woo JA, Ryu H, Kang DE. Cooperative role of RanBP9 and P73 in mitochondria-mediated apoptosis. Cell Death Dis. 2013;4:e476.
46. Melnikov SV, Soll D, Steitz TA, Polikanov YS. Insights into RNA binding by the anticancer drug cisplatin from the crystal structure of cisplatin-modified ribosome. Nucleic Acids Res. 2016;44:4978–87.
47. Belyi VA, Ak P, Markert E, Wang H, Hu W, Puzio-Kuter A, et al. The origins and evolution of the p53 family of genes. Cold Spring Harb Perspect Biol. 2010;2:a001198.
48. Takahasi KR, Sakuraba Y, Gondo Y. Mutational pattern and frequency of induced nucleotide changes in mouse ENU mutagenesis. BMC Mol Biol. 2007;8:52.
49. Simon MM, Moresco EM, Bull KR, Kumar S, Mallon AM, Beutler B, et al. Current strategies for mutation detection in phenotype-driven screens utilising next generation sequencing. Mamm Genome. 2015;26:486–500.
50. Kong A, Frigge ML, Masson G, Besenbacher S, Sulem P, Magnusson G, et al. Rate of de novo mutations and the importance of father's age to disease risk. Nature. 2012;488:471–5.
51. Shultz LD, Lyons BL, Burzenski LM, Gott B, Chen X, Chaleff S, et al. Human lymphoid and myeloid cell development in NOD/LtSz-scid IL2R gamma null mice engrafted with mobilized human hemopoietic stem cells. J Immunol. 2005; 174:6477–89.
52. Lan ZJ, Xu X, Cooney AJ. Differential oocyte-specific expression of Cre recombinase activity in GDF-9-iCre, Zp3cre, and Msx2Cre transgenic mice. Biol Reprod. 2004;71:1469–74.
53. Qiu Z, Cang Y, Goff SP. Abl family tyrosine kinases are essential for basement membrane integrity and cortical lamination in the cerebellum. J Neurosci. 2010;30:14430–9.
54. Ryder E, Gleeson D, Sethi D, Vyas S, Miklejewska E, Dalvi P, et al. Molecular characterization of mutant mouse strains generated from the EUCOMM/KOMP-CSD ES cell resource. Mamm Genome. 2013;24:286–94.
55. Rodriguez CI, Buchholz F, Galloway J, Sequerra R, Kasper J, Ayala R, et al. High-efficiency deleter mice show that FLPe is an alternative to Cre-loxP. Nat Genet. 2000;25:139–40.
56. Kim SY, Ebbert K, Cordeiro MH, Romero M, Zhu J, Serna VA, et al. Cell autonomous phosphoinositide 3-kinase activation in oocytes disrupts normal ovarian function through promoting survival and overgrowth of ovarian follicles. Endocrinology. 2015;156:1464–76.
57. Terakawa J, Rocchi A, Serna VA, Bottinger EP, Graff JM, Kurita T. FGFR2IIIb-MAPK activity is required for epithelial cell fate decision in the lower mullerian duct. Mol Endocrinol. 2016;30:783–95.
58. Nair AB, Jacob S. A simple practice guide for dose conversion between animals and human. J Basic Clin Pharm. 2016;7:27–31.